INSTITUTE OF PHYSICS PUBLISHING SMART MATERIALS AND STRUCTURES
Smart Mater. Struct. **14** (2005) 1377–1386 doi:10.1088/0964-1726/14/6/030

Utilization of embedded optical fibre sensors for delamination characterization in composite laminates using a static strain method

Hang-yin Ling[1,3], **Kin-tak Lau**[1], **Li Cheng**[1] **and Wei Jin**[2]

[1] Department of Mechanical Engineering, The Hong Kong Polytechnic University, Hong Kong, People's Republic of China
[2] Department of Electrical Engineering, The Hong Kong Polytechnic University, Hong Kong, People's Republic of China

E-mail: carrie.lhy@polyu.edu.hk

Received 17 February 2005, in final form 24 August 2005
Published 31 October 2005
Online at stacks.iop.org/SMS/14/1377

Abstract
Embedded fibre Bragg grating (FBG) sensors are utilized to characterize a delamination in glass fibre-reinforced epoxy (GF/EP) composite laminates using a static strain method. Composite beams with different edge delaminations in the thickness-wise direction are monitored by the FBG sensors, whose centres are located at delamination tips of the beams, under a three-point bending test. A surface bonded strain gauge is employed to calibrate the FBG sensor using the bending test. Moreover, strain distribution within the sensing region of the delaminated composite beams is numerically calculated by the finite element method (FEM). FEM results establish the relationship between the strain distribution of the beams and the shape of reflection spectra from the FBG sensors. A correlation between delamination location in the thickness-wise direction of the beams and the shape of the reflection spectra is then highlighted.

(Some figures in this article are in colour only in the electronic version)

1. Introduction

Fibre-reinforced polymer composites have been extensively utilized in marine, aerospace and infrastructure applications as they advance in comparably high specific strength to weight ratio and excellence corrosion resistance. However, damage in the composites is readily induced during their fabrication process and by a low velocity impact with foreign objects. Therefore, damage detection of composite structures is very important to ensure structural integrity and safety. Since delamination, a kind of destructive damage found only in composites, cannot be detected visually, conventional non-destructive evaluation (NDE) techniques such as x-rays, thermography, eddy currents and ultrasonic C-scans have been employed for delamination detection. However, these techniques are not only time consuming, costly and requiring direct human accessibility of the structures, but also they cannot provide real-time structural health monitoring of the condition of structures.

Smart composite structures, capable of self-sensing and self-modifying host structural behaviour, have been attracting much attention for the achievement of continuous and *in situ* monitoring of composite structures in the past decade. The main reason is that they can offer on-line damage detection to identify both the damage location and the severity of the damage based on sensor information. Fibre Bragg grating (FBG) sensors have been widely accepted as intrinsic smart sensors in composite structures because of their small physical size, insensitivity to electromagnetic interference, light weight, capability at high temperature and environmentally unfavourable conditions, and multiplexing ability. Zhou and Sim [1] gave a comprehensive review on

[3] Author to whom any correspondence should be addressed.

the use of embedded fibre-optic sensors for damage detection and assessment in composite structures. The principle of the damage detection in the composite structures is based on the ability of the embedded fibre optic sensors to sense the same strain gradient as damaged structures.

Recent studies [2–4] have been conducted to demonstrate the use of fibre-optic sensors for detecting delamination in composite laminates. However, these methods only focused on a vibration-based methodology. The main disadvantage of the vibration-based method is that it is sensitive only to large damage. Since smaller damage may already affect the structural integrity in practice, it is preferable to detect the damage in its initial stage. Physically, stress concentration around the damage may be a good indicator of the occurrence of a small damage [5]. The influence of the strain variation due to the damage in the composite laminates can be directly observed from the raw sensor signals. Responses from the FBG sensors were proven to be sensitive to non-uniform strain distribution along their gauge length [6].

Since non-uniform strain affects the shape of the reflection spectrum from FBG sensors, FBG sensors have been potentially exploited for damage detection in composite structures [7–9]. In these cases, the sensors are located within the region of the non-uniform strain caused by damage. Okabe *et al* [7] applied FBG sensors for the detection of transverse cracks, which cause strain distribution within the gauge length, in carbon fibre reinforced plastic (CFRP) cross-ply laminates. They claimed that the reflection spectrum became broad and had some peaks with an increase of the transverse density in the 90° ply. Takeda *et al* [8, 9] firstly employed small-diameter FBG sensors to quantitatively detect a delamination in CFRP cross-ply laminates. Reflection spectra from the FBG sensors were obtained during the growth of the delamination under a four-point bending test and cyclic loading conditions. The shape of the reflection spectra changed sensitively with the length of the delamination. To our best knowledge, no research has focused on the effect of non-uniform strain, caused by the delamination occurring between different laminate layers in the composite laminates, on the shape of the reflection spectra from the FBG sensors. Moreover, the shape of these reflection spectra may be useful to characterize the delamination location in the thickness-wise direction of the composite laminates.

In this paper, the use of embedded FBG sensors for characterization of a delamination, which occurs between different laminate layers, in ten-ply woven glass fibre composite beams is studied. Firstly, the uniform and non-uniform strain sensing principles of the FBG sensors are briefly reviewed. Static strain distribution of delaminated beams was measured simultaneously by the FBG sensors and strain gauges under a three-point bending test. Reflection spectra from the FBG sensors are characterized in terms of the delamination locations in the thickness-wise direction and the increasing loads. An FEM analysis was conducted for investigating the strain distribution within the gauge length of the FBG sensors. By comparing the FEM results and measured reflection spectra, the correlation between the shape of the reflection spectrum and the delamination location in the thickness-wise direction is discussed.

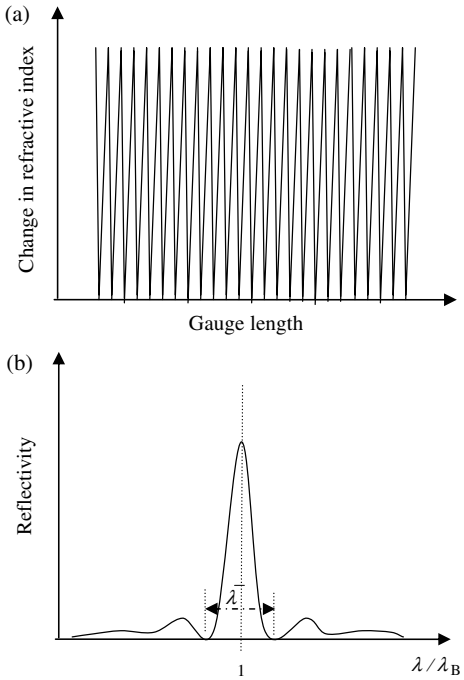

Figure 1. (a) Refractive index variation along the gauge length of a uniform fibre Bragg grating. (b) Corresponding reflection spectrum from a uniform fibre Bragg grating.

2. Strain sensing principle of fibre Bragg grating (FBG) sensors

An optical fibre Bragg grating (FBG), fabricated by UV irradiation of the fibre using the 'phase mask technique', is a permanent periodic modulation in the index of refraction along a given length of the optical fibre core [10]. Figures 1(a) and (b) show refractive index variation along the gauge length of a uniform FBG and the corresponding reflection spectrum, respectively. Bragg wavelength (λ_B, wavelength at maximum reflectivity) and bandwidth ($\bar{\lambda}$, distance between the two first minima) are the two characteristic parameters of this reflection spectrum. Both can be adjusted by changing the parameters of the Bragg grating during the writing process. According to the Bragg law, λ_B is given by

$$\lambda_B = 2n_{\text{eff}}\Lambda \tag{1a}$$

and

$$\frac{\bar{\lambda}}{\lambda_B} = \frac{2\Lambda}{L}, \tag{1b}$$

where Λ is the grating period, L is the gauge length and n_{eff} is the effective mode index of refraction [11].

2.1. Uniform strain sensing

In general, a uniform periodic grating is utilized to determine the strain averaged over the gauge length. For the practical application of the pointwise strain measurement of the structure, this gauge length can be quite short to act as a point sensor. As any changes of strain within the gauge length result in changing of the grating period and the effective mode index of refraction, mechanical strain (ε_g) is determined

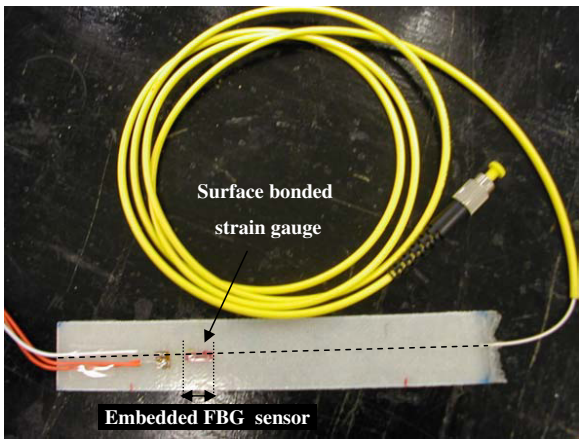

Figure 2. A photograph of the composite beam specimen with the surface bond strain gauge and the embedded FBG sensor.

by measuring the Bragg wavelength shift ($\Delta\lambda_B$). Normally strain transfer to the fibre in transverse directions is very small and can be neglected in practical applications [12]. Also, the temperature effect on the sensor under the temperature controlled environment can also be neglected. Thus, the full equation for the Bragg wavelength shift in term of the effects from the mechanical strain of the fibre within the gauge length is

$$\Delta\lambda_B = K\Delta\varepsilon_g, \tag{2}$$

where K is called the 'theoretical gauge constant' [13], which can be experimentally determined by a calibration test. In general, $\Delta\lambda_B$ can be obtained by an optical spectrum analyser (OSA).

2.2. Non-uniform strain sensing

When a uniform strain is applied along the grating, the shape of the reflection spectrum (a sharp narrow peak) remains the same as the one under its strain-free condition. The reason is that the grating period and effective mode index of refraction are also uniformly changed along the entire gauge length. However, the shape of the reflection spectrum is changed dramatically in an unpredictable manner as the grating is subjected to a non-uniform strain in the longitudinal direction. As the shape of the reflection spectrum strongly depends on the applied non-uniform strain, the FBG sensors show their potential in damage detection. Non-uniform stress concentration, caused by the damage, could be the effective parameter for the damage detection.

For a uniform grating subjected to a non-uniform strain field, it could be treated as a chirped grating problem, in which a chirped grating is subjected to a uniform strain field [14]. The variation of the effective index of refraction of the chirped grating can be written as

$$\eta_{\text{eff}}(x) = \overline{\eta_{\text{eff}}}\left\{1 + \nu\cos\left[\frac{2\pi}{\Lambda_0}z + \phi(z)\right]\right\}, \tag{3}$$

where $\overline{\eta_{\text{eff}}}$ is the mean index change, ν is the fringe visibility of the index change, and $\phi(x)$ describes the change in grating period along the grating [11]. For the case of an applied strain, $\varepsilon_{xx}(x)$, along the longitudinal direction (x-direction), the grating period is

$$\Lambda(x) = \Lambda_0(1 + \varepsilon_{xx}(x)), \tag{4}$$

where Λ_0 is the initial grating period at the strain-free state. According to the previous literature [15],

$$\phi(x) = -\frac{2\pi}{\Lambda_0}\frac{\varepsilon_{xx}(x)}{(1 + \varepsilon_{xx}(x))^2}. \tag{5}$$

Table 1. Corresponding stacking sequences and the normalized values of h_1 and h_2 in different cases.

Case	Stacking sequence	h_1/h	h_2/h
0#	$0^\circ_9/\{OF\}/0^\circ_1$	0 or 1	1 or 0
1#	$0^\circ_1/\{T\}/0^\circ_8/\{OF\}/0^\circ_1$	0.9	0.1
2#	$0^\circ_2/\{T\}/0^\circ_7/\{OF\}/0^\circ_1$	0.8	0.2
3#	$0^\circ_3/\{T\}/0^\circ_6/\{OF\}/0^\circ_1$	0.7	0.3
4#	$0^\circ_4/\{T\}/0^\circ_5/\{OF\}/0^\circ_1$	0.6	0.4
5#	$0^\circ_5/\{T\}/0^\circ_4/\{OF\}/0^\circ_1$	0.5	0.5
6#	$0^\circ_6/\{T\}/0^\circ_3/\{OF\}/0^\circ_1$	0.4	0.6
7#	$0^\circ_7/\{T\}/0^\circ_2/\{OF\}/0^\circ_1$	0.3	0.7
8#	$0^\circ_8/\{T\}/0^\circ_1/\{OF\}/0^\circ_1$	0.2	0.8

3. Delamination characterization in composite beams under a three-point bending test

Stress concentration around the tip of the delamination in composite beams, with a single edged delamination between different laminate layers, is characterized by FBG sensors in a three-point bending test. An FBG sensor embedded in an intact beam was calibrated by a strain gauge to find out the value of K in equation (2) under a uniform strain measurement. These strain values, calculated in accordance with the Bragg wavelengths and measured directly from the strain gauge, are compared with the FEM results. Finally, the delamination of the beams is characterized by analysing the shape of reflection spectra from the FBG sensors.

3.1. Experiments

Balanced type woven glass fibre-reinforced epoxy (GF/EP) composite laminates with a stacking sequence of $[0^\circ]_{10}$ were fabricated by the hand lay-up method. Since the epoxy is highly susceptible to moisture in its liquid state, the laminates were cured under the controlled temperature (20 °C) and humidity (55%) environment for 24 h. A uniform pressure of 4 kPa was applied on the top of the laminates. To simulate a delamination taken place in the composite laminates, a thin Teflon film with 0.1 mm thickness was inserted between the laminate layers during the fabrication process. Then, rectangular specimens with dimensions 160 mm × 25 mm × 2 mm were cut from the laminates. Single-mode acrylate coated FBG sensors with 10 mm gauge length of 250 and 125 μm in coating and cladding diameters, respectively, were chosen to be embedded into the composite laminates. The FBG sensors were embedded between the ninth and tenth layers, counted from the bottom of the specimens, the composite laminates. A total of nine cases, including specimens with different delamination locations in the thickness-wise direction and one intact specimen, were

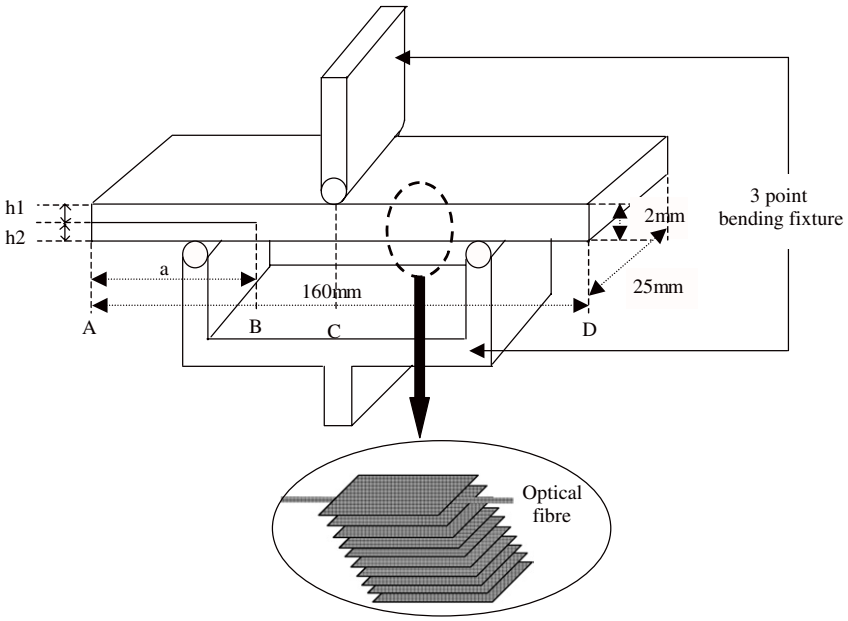

Figure 3. A configuration of a three-point bending test.

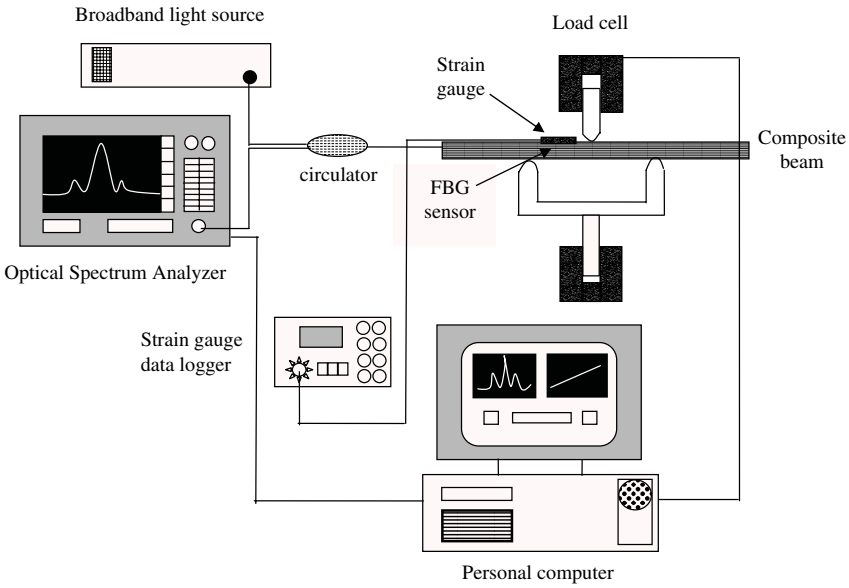

Figure 4. A whole data acquisition system of the experiment in the present study.

tested to investigate the effects of the delamination on a reflection spectrum from the FBG sensor. Table 1 shows the corresponding stacking sequences in different cases. In this table, {OF} and {T} denote the position of the FBG sensor and the delamination, respectively. The positions of a strain gauge and the FBG sensor are illustrated photographically in figure 2. It is important to note that the centre of both sensors was located at the tip of the delamination in order to capture the non-uniform strain distribution around the delamination tip.

Figure 3 presents the configuration of a three-point bending test with a span, $2L$, of 100 mm. Note that a represents the length of the pre-delamination and is equal to 55 mm. h_1 and h_2 denote the thicknesses of the sub-delaminated regions 1 and 2 respectively, and the normalized values of h_1 and h_2 in different cases are listed in table 1. All the tests were performed using an MTS static axial loading test machine. The specimens were loaded under a constant displacement rate of 1 mm min^{-1}. For a calibration test, strain variation was recorded by a strain gauge with averaged static strain and the FBG sensors with the reflection spectra in every extension interval with 0.5 mm simultaneously. For delamination characterization, only the FBG sensors were used to monitor the delaminations of the beams. The whole data acquisition system of this experiment is illustrated schematically in figure 4.

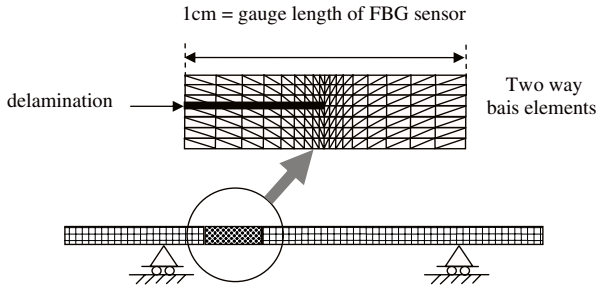

Figure 5. A finite element model for calculation of strain distribution in a delaminated beam.

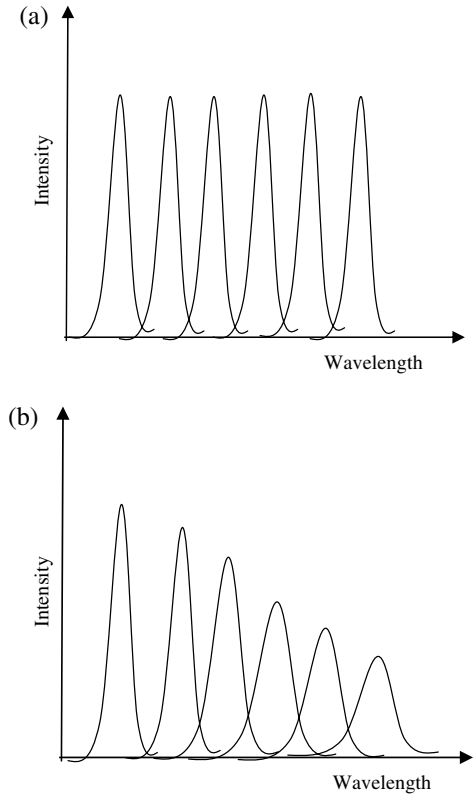

Figure 6. (a) Reflection spectra from the FBG sensor subjected to various tensile loads. (b) Reflection spectra from the FBG sensor subjected to various bending loads.

3.2. FEM analysis

A FEM analysis, performed by an MSC visual Nastran/ Patran commercial software package, was carried out to calculate the theoretical strain distribution at the tip of the delamination while the beam was subjected to a three-point loading. For the beam with a full-width edged delamination, it is reasonable to assume that the material properties are constant in the width-wise direction. A 2D FE model, depicted graphically in figure 5, was chosen to model the delaminated beam under the three-point loading in the present study. Moreover, the effects of the embedded optical fibre are neglected in this preliminary study although these effects cannot be ignored under some situations [16]. The mesh was generated using six-noded triangular finite elements. Two way bias elements, as shown in figure 5, were selected in the region near the

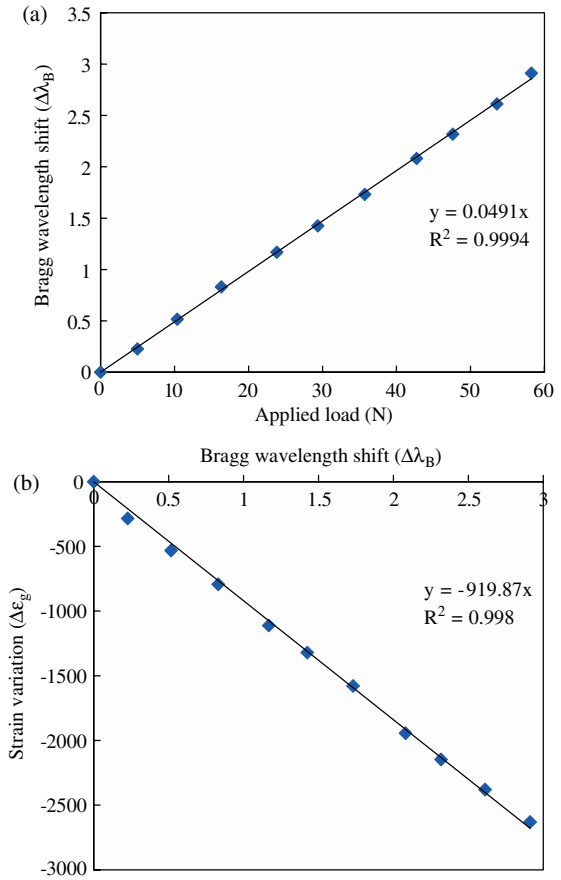

Figure 7. (a) Bragg wavelength shift against the applied load in a calibration test using a three-point bending fixture. (b) Strain variation against Bragg wavelength shift in a calibration test using a three-point bending fixture.

delamination tip to capture the fine strain variation. A total of 7982 nodes and 3401 elements were used in this model. Linear elastic properties for the GF/EP composite were assumed, with the elastic modulus of 15 GPa and Poisson ratio of 0.14. Additionally, the delamination was modelled by assuming its thickness to be 5% of the beam thickness, the elastic modulus of 0.1 GPa and the Poisson ratio of 0.4. The beams with different delaminations were configured by moving the delaminated region along the thickness-wise direction of the beam.

4. Experimental results and discussion

4.1. FBG sensor calibration

The three-bending test, instead of a standard tensile test, was firstly conducted, to calibrate the FBG sensor in this study. In the case of the embedded FBG sensor in the specimen subjected to a tensile load in its spanwise direction, the reflection spectra from the FBG sensor under different loads are sketched in figure 6(a). It is known that the level of the intensity, the shape and the bandwidth of the reflection spectrum still remain the same even under various loads; only the shift of the Bragg wavelength is noticed. The reflection spectrum of the FBG sensor subjected to different loads under the three-point bending fixture is indicated in figure 6(b). The changes of the level of intensity and bandwidth of the spectrum, and also the

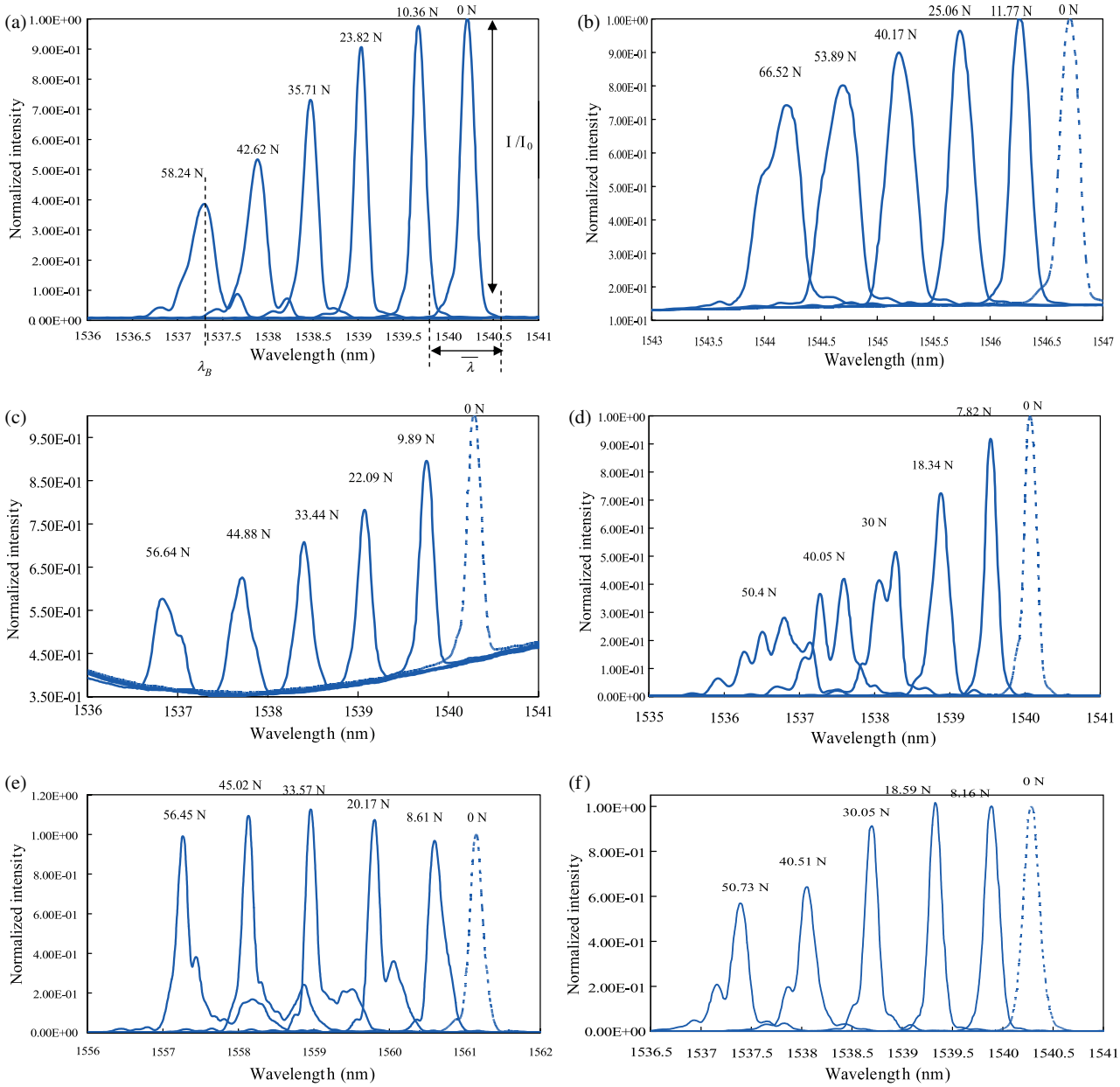

Figure 8. (a) Reflection spectra from the FBG sensor with increasing applied load in case 0#. (b) Reflection spectra from the FBG sensor with increasing applied load in case 1#. (c) Reflection spectra from the FBG sensor with increasing applied load in case 2#. (d) Reflection spectra from the FBG sensor with increasing applied load in case 3#. (e) Reflection spectra from the FBG sensor with increasing applied load in case 4#. (f) Reflection spectra from the FBG sensor with increasing applied load in case 5#. (g) Reflection spectra from the FBG sensor with increasing applied load in case 6#. (h) Reflection spectra from the FBG sensor with increasing applied load in case 7#. (i) Reflection spectra from the FBG sensor with increasing applied load in case 8#.

shift of Bragg wavelength, are observed. These changes of the intensity and bandwidth can be explained by a uniform strain gradient along the grating and resulted in the attenuation of the intensity and increase in bandwidth of the spectrum with increasing load. However, the Bragg wavelength shift still mainly depends on the average of this linear strain distribution. As a result, the FBG sensors can be calibrated by the strain gauge which is able to record the average strain using the three-point bending test.

The Bragg wavelength shift against the applied load in the three-point bending test is shown in figure 7(a). A linear correlation between the Bragg wavelength shift and the applied load is observed. Strain variation due to the applied load was recorded by the strain gauge, and is plotted against the Bragg wavelength shift as depicted in figure 7(b). From this figure, the value of K^{-1} was calculated by a fitting curve as 919.87 for the FBG sensor whose Bragg wavelength at the strain-free state is 1540.2095 nm. This implies that each 1 nm shift of Bragg wavelength corresponds to 919.89 $\mu\varepsilon$ variation of strain. Equation (2) can be converted into

$$\Delta\varepsilon_{\mathrm{g}} = 919.87\Delta\lambda_{\mathrm{B}}. \tag{6}$$

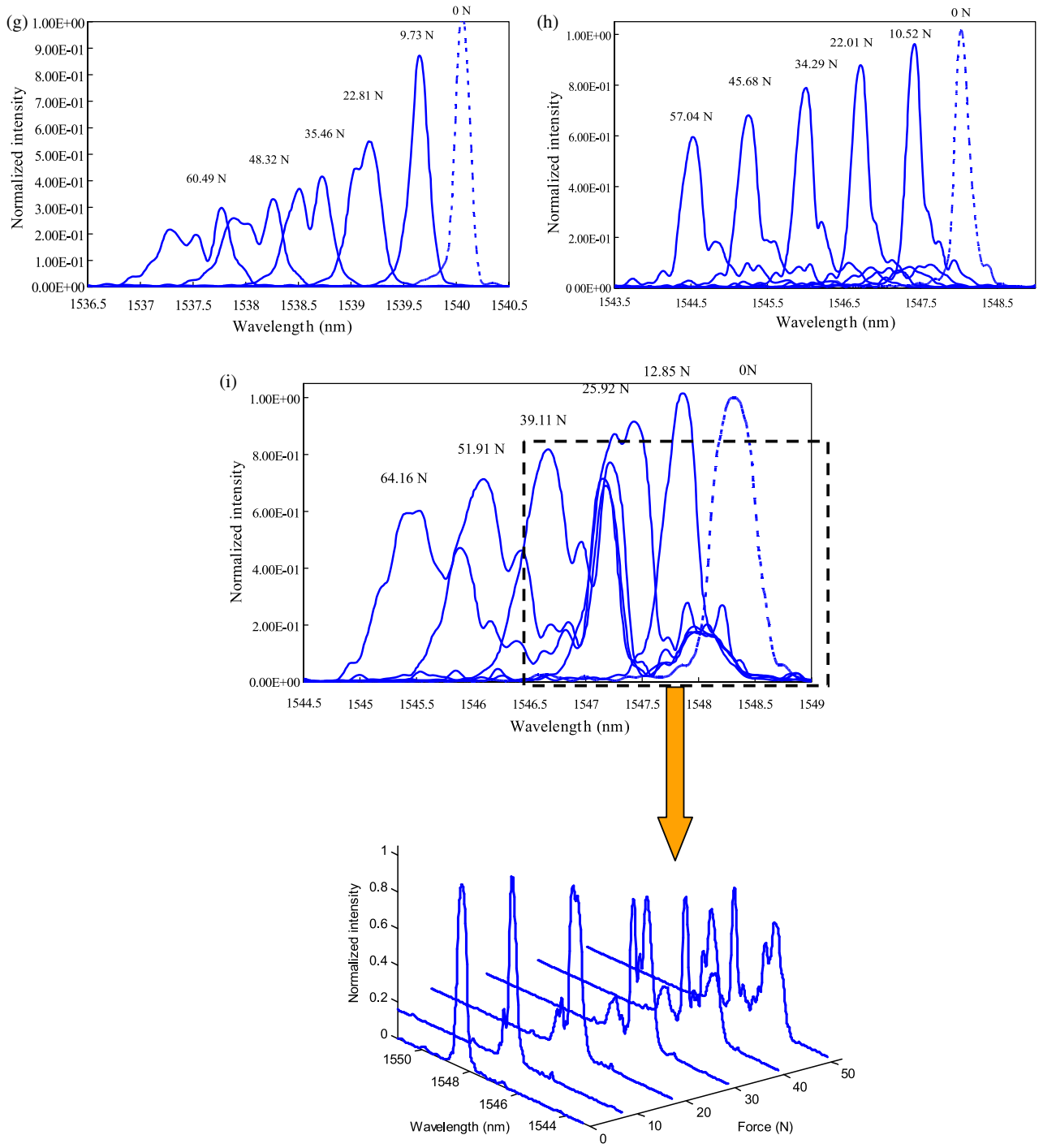

Figure 8. (Continued).

4.2. Delamination characterization

4.2.1. Reflection spectra from FBG sensors. Reflection spectra from the FBG sensors in different delaminated cases through the three-point bending tests are illustrated in figures 8(a)–(i). Generally, obvious changes in the spectral parameters, in terms of level of intensity (I), Bragg wavelength (λ_B) and spectral span (S_p), are observed. Note that S_p is the span of the spectrum and it is equal to λ_B for the spectrum without distortion. Figures 9 and 10 are plotted based on the results of the reflection spectra to quantify the relationship of the applied load and the variations of normalized intensity ($I_N = I/I_0$) and spectral span ($S_{pN} = S_p/S_{p0}$).

Referring to the reflection spectra shown in figures 8(a)–(i), the Bragg wavelength shifts to the left-hand side in all cases because the FBG sensors experienced compressive strain under the bending of the specimens. Moreover, deformation of the reflection spectra is observed while the applied load is getting greater. It is pertinent to note that when the applied load increases, the multiple peaks appear in cases 3#, 4#, 6#, 7# and

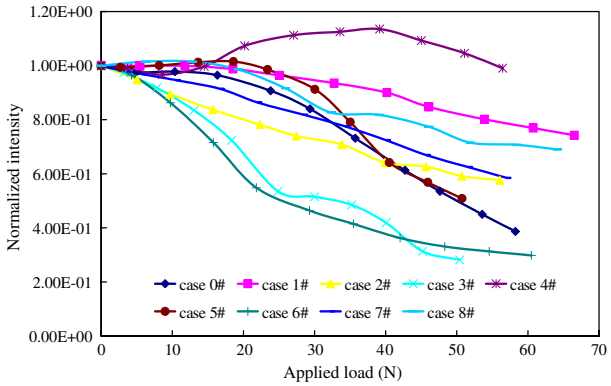

Figure 9. Normalized intensity of the reflection spectra from FBG sensors against applied load in various cases.

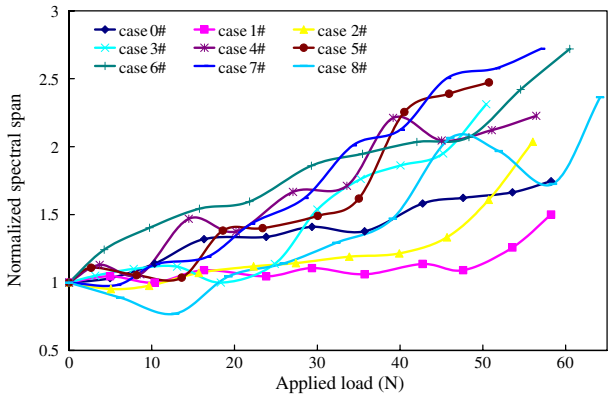

Figure 10. Normalized spectral span of reflection spectra from FBG sensors against applied load in various cases.

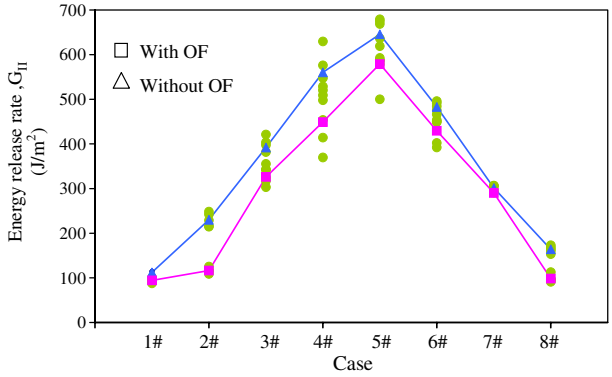

Figure 11. A graph of the mode II energy release rate of the specimens with and without embedded optical fibres in different cases [16].

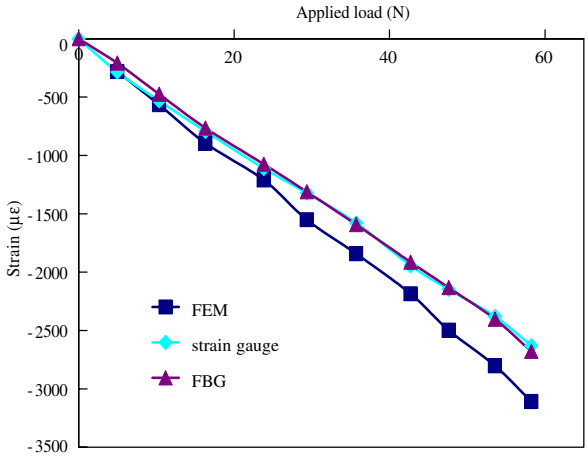

Figure 12. An average strain value of an intact beam along the corresponding gauge length, calculated by FEM and measured using strain gauge and FBG sensors, with increasing applied load.

8#. A correlation between the non-uniform strain distribution caused by the delamination within the gauge length and the spectral parameters will be discussed in the next section.

In most cases, the normalized intensity gradually decreases with the increasing applied load except for cases 4#, 5# and 8#, as indicated in figure 9. This figure shows the normalized intensity slightly increases and then decreases back to the value in the strain-free state. A slight increase and a decrease in the intensity are found in cases 4# and 5#. To explain this phenomenon, figure 11 has been reproduced from [15]. In this figure, it is observed that the mode II energy release rate is the highest in case 5# followed by case 4#. The higher the mode II energy release rate is, the more stable crack propagation is. This fluctuation of the intensity may probably be due to the growth of the delamination since the crack propagation may interrupt the strain gradient along the grating. In case 8#, an increase in the intensity at the beginning may be caused by the effects of an embedded optical fibre. The existence of the optical fibre would guide the crack growth steadily, resulting in the interference on the strain gradient.

In addition, the normalized spectral span increases unstably with the increasing applied load in all cases, except for case 8#, in accordance with figure 10. This fluctuant manner is due to the distortion of the spectrum. More obvious distortion would broaden the spectral span since the total light intensity of the spectrum remains the same for all spectra in each case. Especially for cases 8#, its spectral span slightly decreases at the beginning of the test and rises afterward. This can be explained by the abnormal form of the spectra compared with other cases and it will be further discussed later.

4.2.2. Non-uniform strain distribution found by FEM. The strain distribution of the intact beam along the corresponding gauge length obtained from the FEM and experiments recorded by the strain gauges and the FBG sensors is shown in figure 12. It is noticed that the strain values measured by the strain gauge and the FBG sensor, and numerically calculated by the FEM, are linearly proportional to the applied load. A slightly discrepancy is found in the results from the FEM compared with that from the strain gauge and the FBG sensor. This discrepancy may result from the attenuation of measured strain caused by the adhesive layer of the surface bonded strain gauge, as well as the presence of a protective coating and an adhesive layer of the FBG sensor.

Strain distribution along the grating region of the delaminated beams with various applied loads calculated from the FEM is selectively depicted in figures 13(a)–(c). Figures 13(a)–(c) correspond to cases 0#, 5# and 8#. As

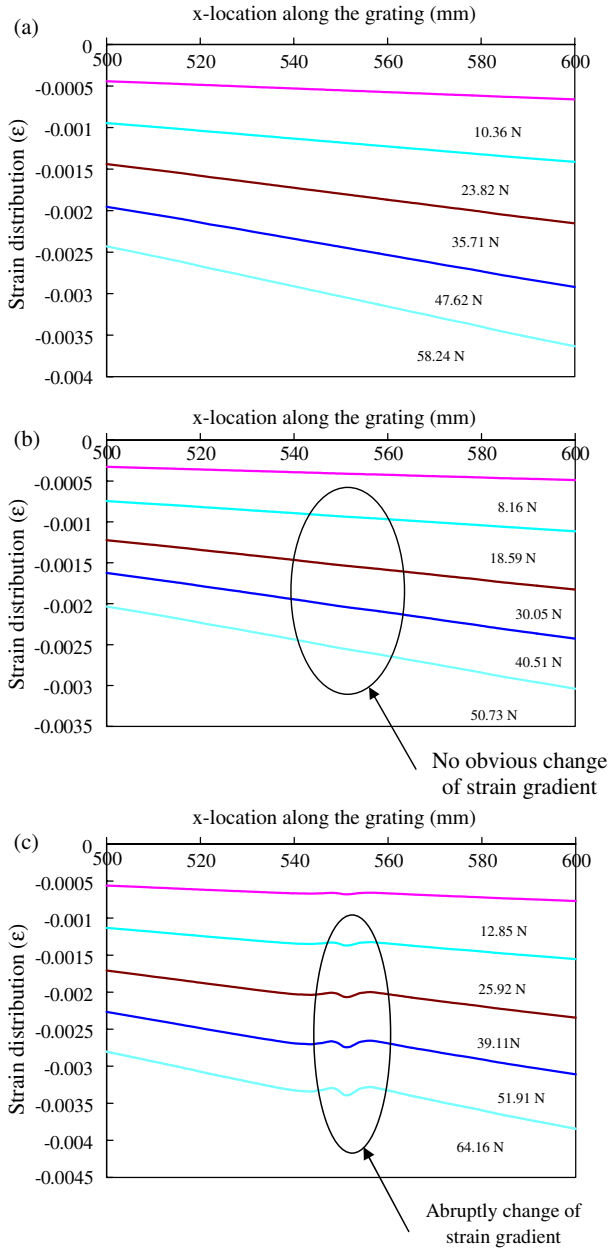

Figure 13. (a) Strain distribution along the grating region with various applied loads based on the calculation from FEM in case 0#. (b) Strain distribution along the grating region with various applied loads based on the calculation from FEM in case 5#. (c) Strain distribution along the grating region with various applied loads based on the calculation from FEM in case 8#.

seen in these figures, the strain gradient gradually increases with the increasing load. This phenomenon can be explained by the bending effect within the gauge length. For the strain distribution of the intact beam, as noticed in figure 13(a), only the shift of Bragg wavelength is observed in the reflection spectrum when the strain gradient is nearly uniform for 10.36 N applied load. This implies that the uniform strain would only cause the shift of Bragg wavelength. However, the intensity decreases while the spectral span increases, as the strain gradient is greater. Consequently, the change in strain gradient of the beam can be indicated by the change of the

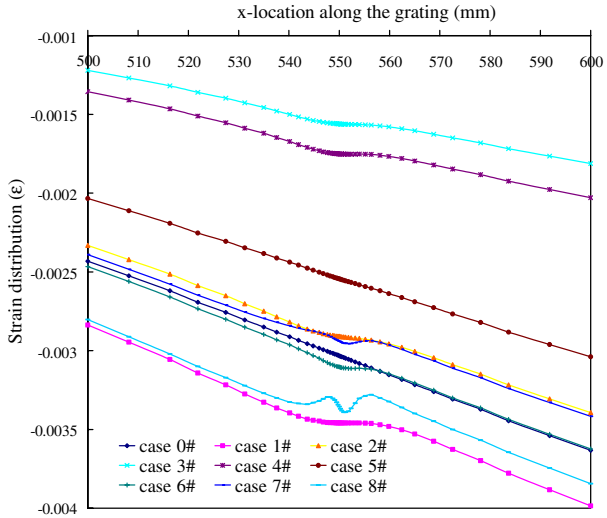

Figure 14. Strain distribution along the grating region with various applied loads based on the calculation from FEM in different cases.

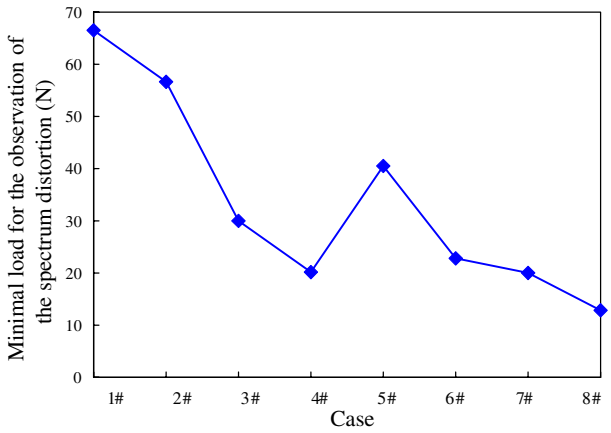

Figure 15. The minimal load for the observation of spectrum distortion in various cases.

intensity and the spectral span shown in the reflection spectrum of the FBG sensor, as shown in figure 8(a).

As mentioned, the presence of the delamination can be identified by the stress concentration at the delamination tip. The greater the bending load is, the larger the stress concentration is. This characteristic is confirmed by the FEM results shown in figure 13(c). The abrupt changes of strain distribution at the location of the delamination tip are noted in this figure. Such changes become apparent with the increasing applied load. However, such changes are not observed in case 5# as seen in figure 13(b).

To further investigate the variation of the strain due to the delamination in different cases, the strain distributions at the highest applied load are plotted in figure 14. Surprisingly, the severity of the strain variation increases from cases 1# to 4#. However, no sudden change in strain is noticed in case 5#. The strain variation becomes obvious again from cases 6# to 8#. For cases 1# to 4#, as well as case 6#, the shape of the strain variation is a flattened line. In contrast, a sine curve shape is seen in cases 7# and 8#. Interestingly, these abrupt changes in the strain distribution are highly correlated with

the minimal load for the observation of spectrum distortion, as seen in figure 15. This implies that more abrupt strain variation would cause spectrum deformations at the earlier stage of the test. By observing the form of the reflection spectrum, the severity of the stress concentration at the delamination tip can be implicated. It is noted that such stress concentration is the highest in case 8#. The stress concentration increases from cases 1# to 4# and drops suddenly in case 5#. Finally, it rises gradually again from cases 6# to 8#. Theoretically, the non-uniform strain distribution along the grating caused by the delamination would lead to variations of the effective mode index of reflection and the grating period, resulting in the distortion of the spectrum. It is concluded that the severity of the deformation of the reflection spectrum becomes greater when the delamination is close to the mid-plane of the beam or the position of the embedded optical fibre.

From figure 8(i), it is important to note that, with loading, the shape of the reflection spectrum is fully distorted compared with the strain-free one. The form of the reflection spectra in case 8# is quite different from the one found in other cases. The greatest distortion of the reflection spectra observed in case 8# is understandable. However, there are two dominant peaks; one remains stagnant with the increasing load; in each reflection spectrum these are abnormally observed. There are two possible explanations for this phenomenon. Firstly, the part of the grating above the delaminated region is free from the strain and corresponds to the unmoving peak, and the part of the grating above the intact region is affected by the compressive strain and corresponds to the peak that shifts to the shorter wavelength side. Moreover, this abnormal change of the reflection spectra can also be explained by an interaction between the embedded optical fibre and the delamination of the specimens. This interaction may cause the interfacial shear strain between the optical fibre and matrix, resulting in the stagnant peak observed in the spectrum.

5. Conclusion

Delaminations in the woven composite laminates were characterized by using the embedded FBG sensors and the three-point bending test. An analysis of the reflection spectra from the FBG sensors, whose centre was embedded at the tip of the delamination, with increasing load showed the dependent relationship between the delamination location and the strain distribution along the gauge length. It was found that the bandwidth and the level of intensity of the reflection spectra highly depend on the strain gradient along the grating. Moreover, the shift of the Bragg wavelength was induced by the average strain along the grating provided that the strain gradient is constant. The abrupt change in the strain gradient caused by the delamination caused the deformation of the reflection spectra. This deformation is more apparent when the applied load is high or the delamination is close to the mid-plane of the beam or the position of the embedded sensor. Especially, the part of the grating free from strain above the delamination and the interfacial shear strain can significantly affect the strain distribution recorded by the FBG sensor when the delamination is positioned just a lamina below the location of the sensor. The future work will focus on quantitative determination of the delamination location in the thickness-wise direction of the composite laminates by using the embedded FBG sensors.

Acknowledgment

This project was supported by The Hong Kong Polytechnic University grant A-PF34.

References

[1] Zhou G and Sim L M 2002 Damage detection and assessment in fibre-reinforced composite structures with embedded fibre optic sensors—review *Smart Mater. Struct.* **11** 925–39
[2] Bhatia V, Schmid C A, Murphy K A, Claus R O, Tran T A, Greene J A and Miller M S 1995 Optical fiber sensing technique for edge-induced and internal delamination detection in composites *Smart Mater. Struct.* **4** 164–9
[3] Watkins S E, Sanders G W, Akhavan F and Chandrashekhara K 2002 Modal analysis using fibre optic sensors and neural networks for prediction of composite beam delamination *Smart Mater. Struct.* **11** 489–95
[4] Ling H Y, Lau K T, Cheng L and Jin W 2005 Fibre optic sensors for delamination identification in composite beams using genetic algorithm *Smart Mater. Struct.* **14** 287–95
[5] Huang S, Ohn M M, LeBlanc M and Measure R M 1998 Continuous arbitrary strain profile measurements with fiber Bragg gratings *Smart Mater. Struct.* **7** 248–56
[6] Peters K, Pattis P, Botsis J and Giaccari P 2000 Experimental verification of response of embedded optical fiber Bragg grating sensors in non-homogeneous strain fields *Opt. Lasers Eng.* **33** 107–19
[7] Okabe Y, Yashiro S, Kosaka T and Takeda N 2000 Detection of transverse cracks in CFRP composites using embedded fiber Bragg grating sensors *Smart Mater. Struct.* **9** 832–8
[8] Takeda S, Okabe Y and Takeda N 2002 Delamination detection in CFRP laminates with embedded small-diameter fiber Bragg grating sensors *Composites* A **33** 971–80
[9] Takeda S, Okabe Y, Yamamoto T and Takeda N 2003 Detection of edge delamination in CFRP laminates under cyclic loading using small-diameter FBG sensors *Compos. Sci. Technol.* **63** 1885–94
[10] Othonos A and Kalli K 1999 *Fiber Bragg Gratings: Fundamentals and Applications in Telecommunications and Sensing* (Boston: Artech House)
[11] Erdogan T 1997 Fiber grating spectra *J. Lightwave Technol.* **15** 1277–94
[12] Maaskant R, Alavie T, Measures R M, Tadros G, Rizkalla S H and Guhathakurta A 1997 Fiber-optic Bragg grating sensor for bridge monitoring *J. Cement Concrete Compos.* **19** 21–33
[13] Udd E 1995 *Fiber Optic Smart Structures* (New York: Wiley)
[14] Saouma V E, Anderson D Z, Ostrander K, Lee B and Slowik V 1998 Application of fibre Bragg grating in local and remote infrastructure health monitoring *J. Mater. Struct.* **31** 259–66
[15] Peters K and Studer M 1999 Measurement of stress concentrations using embedded optical fiber Bragg garting sensors *SPIE Sensory Phenom. Meas. Instrum. Smart Struct. Mater.* **3670** 195–206
[16] Ling H Y, Lau K T and Lam C K 2005 Effects of embedded optical fibre on mode II fracture behaviours of woven composite laminates *Composites* B **36** 534–43